AIP | Review of Scientific Instruments

A time-of-flight backscattering spectrometer at the Spallation Neutron Source, BASIS

E. Mamontov and K. W. Herwig

Citation: Review of Scientific Instruments **82**, 085109 (2011); doi: 10.1063/1.3626214
View online: http://dx.doi.org/10.1063/1.3626214
View Table of Contents: http://scitation.aip.org/content/aip/journal/rsi/82/8?ver=pdfcov
Published by the AIP Publishing

A time-of-flight backscattering spectrometer at the Spallation Neutron Source, BASIS

E. Mamontov[a] and K. W. Herwig
Neutron Scattering Science Division, Oak Ridge National Laboratory, Oak Ridge, Tennessee 37831, USA

(Received 1 June 2011; accepted 28 July 2011; published online 25 August 2011)

We describe the design and current performance of the backscattering silicon spectrometer (BASIS), a time-of-flight backscattering spectrometer built at the spallation neutron source (SNS) of the Oak Ridge National Laboratory (ORNL). BASIS is the first silicon-based backscattering spectrometer installed at a spallation neutron source. In addition to high intensity, it offers a high-energy resolution of about 3.5 μeV and a large and variable energy transfer range. These ensure an excellent overlap with the dynamic ranges accessible at other inelastic spectrometers at the SNS. © *2011 American Institute of Physics*. [doi:10.1063/1.3626214]

I. INTRODUCTION

The time-of-flight neutron scattering spectrometers utilize either direct scattering geometry, when the initial energy of the neutrons incident on the sample, E_i, is selected by a monochromator or choppers, or inverted scattering geometry, when the final energy of the neutrons scattered by the sample, E_f, is selected by the analyzer crystals. The technique known as backscattering[1,2] is the limiting case of the inverted scattering geometry that utilizes energy analyzer crystals with a fixed Bragg reflection angle at or near 90°. This geometry minimizes the energy resolution of the analyzer according to the following expression:

$$\delta E_f = 2E_f\left(\frac{\delta d}{d} + \cot\theta\delta\theta\right), \quad (1)$$

which can be easily obtained by differentiating Bragg's law. Here $\delta d/d$ is the spread of the analyzer lattice constant, and θ is the Bragg angle; the second terms in the bracket is minimized when θ approaches 90° (thus the term "backscattering"). Neutron backscattering spectrometry is characterized by a high energy resolution, often on the energy scale of μeV. The scattering at such low energy transfers probes dynamic processes on the nano-second time scale. In typical neutron time-of-flight experiments, much faster processes on the pico-second time scale are usually probed, whereas neutron spin-echo can be used to probe much slower processes on the tens and hundreds of nano-seconds time scale. Neutron backscattering can thus bridge the gap between the time scales probed in neutron time-of-flight and spin-echo experiments. The precision with which the neutron energy transfer, $E = E_i - E_f$, can be determined (that is, the overall energy resolution) depends on accurate knowledge of both the initial energy, E_i, and the final energy, E_f. The precision of the latter is determined mainly by the analyzer crystals type and arrangement according to Eq. (1); utilization of the backscattering geometry when θ is near 90° minimizes the spread in the measured E_f. Most backscattering spectrometers have been built at neutron research reactors that provide continuous beam, where some kind of a monochromator is needed to set up the E_i for the neutrons incident on the sample. The variation of the E_i is then achieved by means of either varying the temperature of the monochromator with respect to that of the analyzer, thereby changing the lattice constants of the monochromator and the E_i,[3] or Doppler-moving the monochromator.[4] The latter approach requires much shorter measurement times and is usually adopted, even though the former approach allows measurements over much larger dynamic range not limited by the range of the Doppler-driven monochromators. In either case, the spread in E_i is determined by the monochromator, and is typically similar to the spread in the E_f. This can yield a sub-μeV overall energy resolution at a reactor-based backscattering spectrometer, such as IN10 and IN16 at the ILL, France,[5] HFBS at the NCNR, USA,[6] and SPHERES at the FRM-II, JCNS, Germany.[7] At the same time, these backscattering spectrometers suffer from the somewhat limited dynamic range achievable with Doppler-driven monochromators (presently, some ±30–35 μeV at best). These spectrometers use silicon analyzer crystals and monochromators, where the $\delta d/d$ is controlled by introducing elastic deformation of the crystals. The perfect backscattering geometry ($\theta = 90°$) employed at these spectrometers requires detector positioning in the horizontal plane behind the sample (that is, the neutrons pass through the sample twice on their way to the detectors).

The time-of-flight (TOF) backscattering spectrometers (TOF-BSS) typically built at spallation neutron sources do not use monochromators; instead, the neutron's E_i is determined from the overall time-of-flight between the neutron source and the detectors. The dynamic range is limited only by the frame overlap, and is determined by the combination of the source repetition rate, neutron flight path distances, and choice of the bandwidth-limiting choppers. Energy transfers of several hundred μeV are easily achievable. The energy resolution, however, is coarser compared to that of the reactor-based backscattering spectrometers. To the first

[a] Author to whom correspondence should be addressed. Electronic mail: mamontove@ornl.gov. Telephone: 1-865-5745109. FAX: 1-865-574-6080.

approximation, it can be written as

$$\delta E = 2E\sqrt{\left(\frac{\delta d}{d} + \cot\theta\delta\theta\right)^2 + \left(\frac{\delta \mathrm{TOF}}{\mathrm{TOF}}\right)^2}. \quad (2)$$

The problem is that it is difficult to reduce the time-of-flight term, which decreases with the increasing flight path distances, below certain, economically feasible limit. It is often more practical to intentionally coarsen the other term in order to match the contribution from the time-of-flight term, thus increasing the signal intensity without degrading the resolution much. While a TOF-BSS built on spallation neutron sources profitably utilizes pulsed structure of the incident neutron beam, its design should find a reasonable balance between the energy resolution, dynamic range, signal intensity, accessible Q-range, etc. Unfortunately, these parameters of merit are often in direct conflict with one another. For instance, high energy resolution is achieved at the expense of signal intensity, longer neutron flight paths improve the resolution but adversely affect the dynamic range, Q-range suffers when analyzer crystals with large d-spacing are used in an attempt to improve the resolution, etc. In practice, it is the primary flight path (moderator to sample) that defines the term δTOF/TOF, because the moderator-to-sample distance is typically much longer compared to the sample-to-analyzer and analyzer-to-detector distances. To match the analyzer resolution to that of the primary flight path, choosing a Bragg angle of 90°, as typical for the reactor-based backscattering spectrometers, is usually impractical for TOF-BSS, as it would require extremely long primary flight path to make the δTOF/TOF term sufficiently small to match the $\delta d/d$ term. In principle, there exists a possibility to use a shorter flight path in conjunction with a pulse-shaping chopper, which could reduce the δTOF term well below the value provided by the moderator; however, this comes at a price of the reduced dynamic range and neutron flux. Thus, relaxing the $\cot\theta\delta\theta$ term through the selection of the near-backscattering Bragg angle (less than 90°) is common for TOF-BSS, but not for the reactor-based backscattering spectrometers. Despite the lower tolerance to the vertical extension of the analyzer panels compared to the true backscattering geometry, the near-backscattering geometry has its advantages. For instance, with the detectors positioned above and below the horizontal scattering plane, detected neutrons do not have to travel through the sample twice, and, therefore, both sides of the instrument tank can be populated with analyzer crystals and detectors. Until recently, practical realizations of TOF-BSS included use of either pyrolytic graphite (PG) or mica analyzer crystals. In both cases, the $\delta d/d$ term is controlled through the selection of the desirable crystal mosaicity. For example, the LAM-80ET spectrometer, built at the KENS, Japan,[8,9] had a primary flight path of about 26 m and used reflections from mica analyzers with an off-backscattering Bragg angle of 80°. In this case, the contribution to the resolution from the $\delta d/d$ term was small compared to that of the $\cot\theta\delta\theta$ term. It has been generally true that mica-based backscattering spectrometers in the past suffered from low intensity problems. For instance, the IRIS spectrometer[10] with a primary flight path of 36.4 m, which was built at the ISIS, UK and is currently in operation, also has mica analyzer crystals; however, its PG analyzers have been used much more often. For the main working reflection, PG (002), $\delta d/d = 0.002$. With the moderator pulse width δTOF ≈ 120 μs, a match between the resolution contributions from the primary and secondary spectrometers was achieved at a near-backscattering Bragg angle of 87.5°. With the analyzers spatially extended in 2000,[11] the current resolution using the PG (002) reflection is 17.5 μeV. The graphite analyzers of the IRIS need to be cryogenically cooled in order to suppress thermal diffuse scattering from graphite. The OSIRIS spectrometer, built at the ISIS more recently[12] and conceptually similar to the IRIS, has a significantly higher flux and somewhat coarser energy resolution of 24.5 μeV with the PG(002) reflection.

With the mica-based TOF-BSS suffering from the low intensity (and a very limited Q-range) and the PG-based TOF-BSS having the energy resolution well above 15 μeV, there has been a need for a TOF-BSS with a higher energy resolution, approaching that of the reactor-based backscattering spectrometers, yet with sufficiently high scattering signal. A new TOF-BSS, BASIS, constructed at the spallation neutron source at Oak Ridge National Laboratory, USA, entered the general user program in the late 2007. This is the first realization of a silicon-based TOF-BSS (hence the name BASIS, which is an acronym for Backscattering Silicon Spectrometer). It features a long primary flight path of 84 m and Si(111) analyzer crystals with $\delta d/d = 0.00035$ at a near-backscattering angle of 88°. Different from the previously built TOF-BSS, the silicon analyzer crystals of the BASIS are near perfect (have no mosaicity); the spread of the silicon lattice parameter is carefully controlled by introducing the elastic deformation of the crystals, similar to the reactor-based silicon backscattering spectrometers. The design and performance of the BASIS are described in detail in the next Sections.

II. SPECTROMETER LAYOUT

The BASIS employs, for the first time in the history of BSS-TOF instruments, Si(111) analyzer crystals, which provides an opportunity for high energy resolution and dictates other spectrometer parameters needed to maintain the overall high resolution. The resolution can be estimated, using the time-of-flight t_i and t_f through the initial (moderator to the sample) and final (sample to the analyzers to the detectors) flight paths, L_i and L_f, and their respective uncertainties, as described below.[13,14] The overall energy resolution is

$$\delta E = \sqrt{\delta E_p^2 + \delta E_s^2}. \quad (3)$$

Here the first term, δE_p, is the contribution from the incident flight path up to the sample,

$$\delta E_p = 2E_i\sqrt{\left(\frac{\delta L_i}{L_i}\right)^2 + \left(\frac{\delta t_0}{t_i}\right)^2}, \quad (4)$$

where δt_0 is moderator emission time width for a specific wavelength. The second term in Eq. (3), δE_s, includes the

contribution from the sample geometry and the final flight path,

$$\delta E_s = 2\sqrt{E_i^2\left(\frac{\delta t_f}{t_i}\right)^2 + E_f^2\left((\cot\theta\delta\theta)^2 + \left(\frac{\delta d}{d}\right)^2\right)}. \quad (5)$$

The term δE_s can be further separated into the contributions from the analyzer crystals,

$$\delta E_a = 2\frac{\delta d}{d}\sqrt{\left(\frac{E_i t_f}{t_i}\right)^2 + E_f^2}, \quad (6)$$

and from the sample size

$$\delta E_{fs} = 2\sqrt{\left(\frac{E_i t_f}{t_i}\frac{\delta L_f}{L_f}\right)^2 + \left(\left(\frac{E_i t_f}{t_i}\right)^2 + E_f^2\right)(\cot\theta\delta\theta)^2}, \quad (7)$$

to give

$$\delta E_s = \sqrt{\delta E_a^2 + \delta E_{fs}^2}. \quad (8)$$

The resolution term from the incident flight path is controlled through maintaining an 84 m distance between the moderator and the sample position and installing the BASIS at the SNS Beamline 2 illuminated by a decoupled supercritical hydrogen centerline-poisoned moderator with the emission time width of about 60 μs for the wavelength of 6.3 Å.

Incident neutrons travel to the sample position through an 83.725 m long supermirror guide; its geometry is described in detail in Table I. In brief, the upstream sections of the guide have a horizontal curvature of 1000 m radius, with the direct line-of-sight ending at about 28 m from the moderator. The curved guide helps eliminate fast neutrons and gamma-rays. At 31 m from the moderator, a straight guide section smoothly joins the curved guide. The coating of the guide sections varies; the last section of the tapered guide has $m = 3.6$. Importantly, the first sections of the guide are placed inside the core vessel and the primary shutter, thereby providing an increased incident neutron flux. The guide has several gaps to accommodate the primary and secondary shutters and bandwidth selection choppers positioned at 7, 9.25, and 50 m from the moderator. Both the curved and straight guide sections have a rectangular cross-section of 12 cm height and 10 cm width at all distances but the last 8 m of the guide, where tapered supermirror sections compress the beam to 3.25 cm by 3.25 cm at the exit of the guide at 27.5 cm upstream the sample position. In fact, a part of the last, funnel section of the guide resides inside the spectrometer tank. A system of slits, vertical and horizontal, which allows restriction of the incident beam size, and the incident beam monitor at 23.4 cm upstream the sample position, are located between the exit of the guide and the sample position. Figure 1 shows a snapshot of the beam at the sample position taken with an image plate, with the slits fully open and not interfering with the beam, and the incident wavelength band centered at 6.3 Å. The divergence of the beam was measured to be slightly above 30 mrad, in both vertical and horizontal directions.

Figure 2 shows the incident spectrum measured at the incident beam monitor (close to the sample position) with the bandwidth selection choppers resting in the open position and the source frequency of 1 Hz, so that the measured time frame width (the interval between the successive neutron pulses) is 1 s, and the frame overlap is completely avoided. The spectrum, which has been normalized to the 1/v efficiency of the monitor, is a product of the moderator output, the guide transmission function, and the absorption in the aluminum windows that the incident beam passes through. During regular operation at the source frequency of 60 Hz, when the time frame width equals 16,667 μs, the choppers must be rotated to eliminate frame overlap and restrict the dynamic range. The BASIS choppers (see Fig. 3) are aluminum disks coated with boron-10 loaded epoxy layer with a transmission of less than 0.001% for 1 Å neutrons, and have open sectors cut in the disks. The open angles are 51.4° for the chopper at 7 m, 57.6° for the chopper at 9.25 m, and 171.1° for the chopper at 50 m. At the source frequency of 60 Hz, phasing the choppers that are rotating at 60 Hz at a desirable value of the wavelength band center results in the incident bandwidth of 0.5 Å with the choppers fully open, regardless of the selected center of the wavelength band. In the quasielastic scattering regime, the choppers are phased to transmit the 0.5 Å bandwidth centered near the Si(111) elastic reflection of 6.267 Å, which provides an energy transfer range of about $\pm$170 μeV. Use of the data collected with the choppers partially open or closed extends the energy transfer range attainable in the quasielastic regime beyond $\pm$200 μeV. Alternatively, the choppers can be operated at a frequency lower than the 60 Hz frequency of the SNS, thereby greatly extending the incident bandwidth (e.g., at 30 Hz, to 1 Å with the choppers fully open). Such an extension, which leads to the concomitant extension of the accessible dynamic range, comes at a price of the reduced intensity due to elimination of some neutron pulses. Regardless of the selected frequency and the bandwidth center of the choppers, it is usually practical to make sure that the transmitted wavelength band includes $\lambda_i = 6.267$ Å, so that the elastic line is present in the measured spectrum.

The spectrometer tank is evacuated down to below 10 mTorr, as required for the detectors operation, and employs extensive background reducing shielding at various locations. The sample chamber, which is typically also evacuated to reduce the background (though it is not required for operation), is separated from the main spectrometer tank by a thin aluminum window. This allows quick replacement of sample environment equipment without breaking vacuum in the main tank. The sample chamber opens at the top of the spectrometer tank, from where the sample environment equipment is installed. After exiting the guide and traveling through the system of slits, the incident beam monitor, and the separation aluminum window, the incident neutrons arrive at the sample position. The neutrons that assume energy of 2082 μeV (wavelength of 6.267 Å) after scattering by the sample can be subsequently Bragg-reflected by the analyzers toward the detectors, as illustrated schematically in Fig. 4. Note that on the way from the sample to the analyzer crystals and back to the detectors, neutrons have to pass through a radial

TABLE I. Description of the BASIS neutron guide system. The numbers show the distance along the guide center measured from the face of the moderator. Other important numbers: Chopper 1 position = 700 cm, Chopper 2 position = 925 cm, Chopper 3 position = 5000 cm, sample position = 8400 cm.

Section	Length (cm)	Interior dimensions	Coating values	Radius of curvature (m)	Notes
Space	120.4	N/A	N/A	N/A	Space between the moderator and the beginning of core vessel section
Core vessel section	105	10 cm horizontal 12 cm vertical	top/bottom/left/right $m = 1$	N/A	Natural Ni on aluminum
Gap	4.3	N/A	N/A	N/A	Gap between core vessel section and shutter guide insert
Shutter guide insert	184.5	10 cm horizontal 12 cm vertical	top/bottom $m = 1.5$ inner radius $m = 1$ (Ni) outer radius $m = 2.5$	1000	
Gap	5.4	N/A	N/A	N/A	Gap between shutter guide insert and first external guide section
Curved guide Section I	274.5	10 cm horizontal 12 cm vertical	top/bottom $m = 1.5$ inner radius $m = 1$ (Ni) outer radius $m = 2.5$	1000	Guide section between target monolith and Chopper 1
Gap	8	N/A	N/A	N/A	Gap for Chopper 1
Curved guide Section II	220	10 cm horizontal 12 cm vertical	top/bottom $m = 1.5$ inner radius $m = 1$ (Ni) outer radius $m = 2.5$	1000	Guide section between Choppers 1 and 2
Gap	5	N/A	N/A	N/A	Gap for Chopper 2
Curved guide Section III	2173	10 cm horizontal 12 cm vertical	top/bottom $m = 1.5$ inner radius $m = 1$ (Ni) outer radius $m = 2.5$	1000	
Straight guide Section I	1897	10 cm horizontal 12 cm vertical	top/bottom $m = 1.5$ sides $m = 1.5$	N/A	Smoothly joins to curved guide Section III
Gap	8	N/A	N/A	N/A	Gap for Chopper 3 followed by secondary shutter
Straight guide Section II	2567.4	10 cm horizontal 12 cm vertical	top/bottom $m = 1.5$ sides $m = 1.5$	N/A	
Funnel guide Section	800	Horizontal: 10 cm at Start, 10 cm over first 150 cm, then tapering uniformly to exit of 3.25 cm taper angle = 5.19 mrad Vertical: 12 cm Vertical at Start Tapering smoothly to 3.25 cm at exit taper angle = 5.47 mrad	Horizontal: sides $m = 1.5$ first 150 cm; $m = 2.5$ next 325 cm; $m = 3.6$ last 325 cm Vertical: top/bottom $m = 2.5$ first 400 cm $m = 3.6$ last 400 cm	N/A	Smoothly joins to straight guide Section II; vertical funnel starts 150 cm prior to horizontal, first halves of each tapered section are $m = 2.5$, second halves are $m = 3.6$.

collimator with a 4° separation between the vertical blades, which restrict the view of the sample and reduces the background.

The analyzer panels inside the BASIS tank are shown in Fig. 5. Presently, one half of the spectrometer tank is populated with 18 Si(111) analyzer crystals that cover about 150° in the horizontal plane and about ±22° in the out-of-plane directions, thus providing a coverage of about 2 sr, or 16% of 4π. An important improvement in the resolution was achieved by using two sets of panels instead of one; the 9 upper and 9 lower spherical panels, split in the middle (in the horizontal plane), as one can see in Figs. 4 and 5. The upper and lower spherical panels have focal points at 9 cm above and below the sample position, respectively, thus reflecting scattered neutrons toward the separate detector banks positioned above and below the horizontal plane. The Si (111) crystals are nearly perfect; thus, the desired $\delta d/d = 0.00035$ is achieved, much like on the reactor-based silicon backscattering spectrometers, by means of elastically straining silicon through press-gluing hexagonal crystal wafers (2 mm thick, 12 cm diagonal) onto the spherical support panels of 2.5 m radius. This is a challenging task since such the large wafer thickness borders the

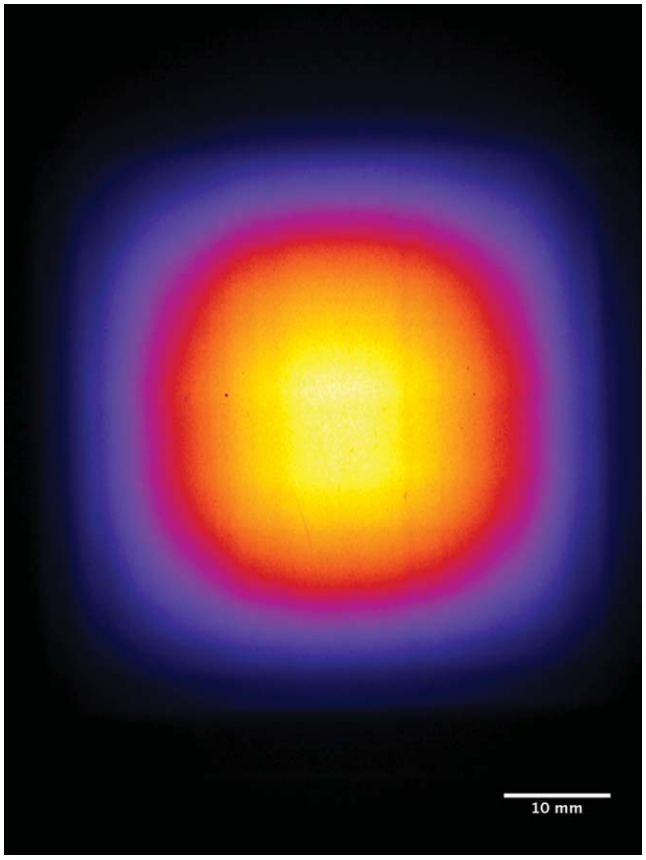

FIG. 1. (Color) Beam image measured at the sample position. The incident wavelength band was centered at 6.3 Å.

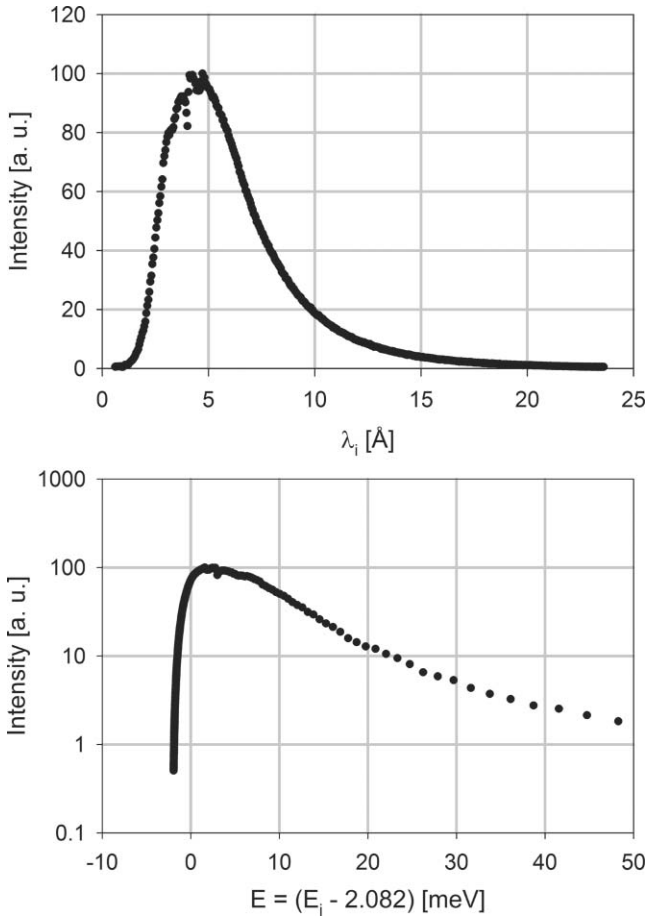

FIG. 2. Efficiency-normalized incident spectrum intensity measured at the incident beam monitor (see the text), plotted as a function of the neutron incident wavelength (top, linear scale) and the energy transfer (bottom, logarithm scale).

breaking limit for silicon material. The Bragg angle of about 88° was selected to nearly match the contributions from the primary and secondary spectrometers. Thus, Bragg-reflected neutrons have a wavelength of 6.267 Å (energy of 2082 μeV).

The top and bottom detector arrays which form circular detector banks above and below the horizontal plane, as shown in Fig. 6, are comprised of 56 linear position-sensitive He-3 tubes each. Each tube has a diameter of 1.25 cm, an active length of 15 cm, and is filled with He-3 at 8 atmospheres. The total flight path from the sample to analyzer crystals to the detectors (see Fig. 4), which includes the constant contribution of 2.5 m from the sample-to-analyzer distance, varies between 4.71 m and 4.729 m around a mean value of 4.72 m, depending on the out-of-plane angle of the neutron scattered by the sample. The variations as a function of the detector pixel height in the flight path and, less importantly, in the Bragg angle and the reflected neutron wavelength, are accounted for in the data reduction software, which converts time-of-flight into energy transfer independently for each detector pixel. Since the exact flight path and the final wavelength are known for each detector pixel (assuming a point sample), the incident energy, and, thus, the energy transfer, $E = E_i - E_f$, can be calculated from the total time-of-flight of the detected neutrons. The value of the scattering momentum transfer, Q, can be calculated in a similar fashion, as $Q = (k_i^2 + k_f^2 - 2k_ik_f\cos(2\theta))^{1/2}$. It is important to note that the implemented detector scheme allows generation of reduced data sets at true constant-Q values. Because of the large accessible energy transfers, this is of greater importance for TOF-BSS compared to reactor-based BSS. The latter typically use the elastic approximation, $k_i = k_f = 2\pi/\lambda$, which yields $Q = Q_{el} = (4\pi/\lambda)\sin(2\theta/2)$; a single Q value defined by the nominal scattering angle is usually assigned to each detector tube. The range of Q and energy transfers accessible on the BASIS as shown in Fig. 7 is calculated from the known values of the scattering angles covered by the analyzer panels and the detectors, which vary between $2\theta_{min} = 11.5°$ and $2\theta_{max} = 161.2°$. In the most often used quasielastic regime of operation, the accessible Q range is between 0.2 and 2.0 Å^{-1}. The accessible range of energy transfers may extend beyond 40 meV, thanks to the fact that incident neutrons with wavelength as low as 1.5 Å are still transmitted by the spectrometer guide system in small, but appreciable numbers. It is important to emphasize that, unlike in the quasielastic regime of operation, the entire Q-ω range shown in Fig. 7 cannot be accessed in one set of measurements. It will require collecting and putting together many data sets measured with different chopper settings of the center of the incident bandwidth to continuously cover the entire Q-ω range shown in Fig. 7. This difficulty is somewhat alleviated by the fact that the energy transfer range accessible with a particular set of chopper

FIG. 3. (Color online) Photograph of one of the BASIS choppers with the cover plate beneath. The aluminum window at the position of the neutron guide is visible at the front.

phasings increases greatly at shorter incident wavelengths (despite the always constant value of $\Delta\lambda_i = 0.5$ Å when the choppers are operated at 60 Hz). This is because the incident energy and energy transfer depend on the incident wavelength in a non-linear manner: $E_i \sim (1/\lambda_i)^2$.

III. SPECTROMETER PERFORMANCE

Currently, efforts are under way to build additional crystal analyzer panels for the presently unpopulated side of the BASIS tank, which may include both the Si(111) panels of improved design and different types of analyzer

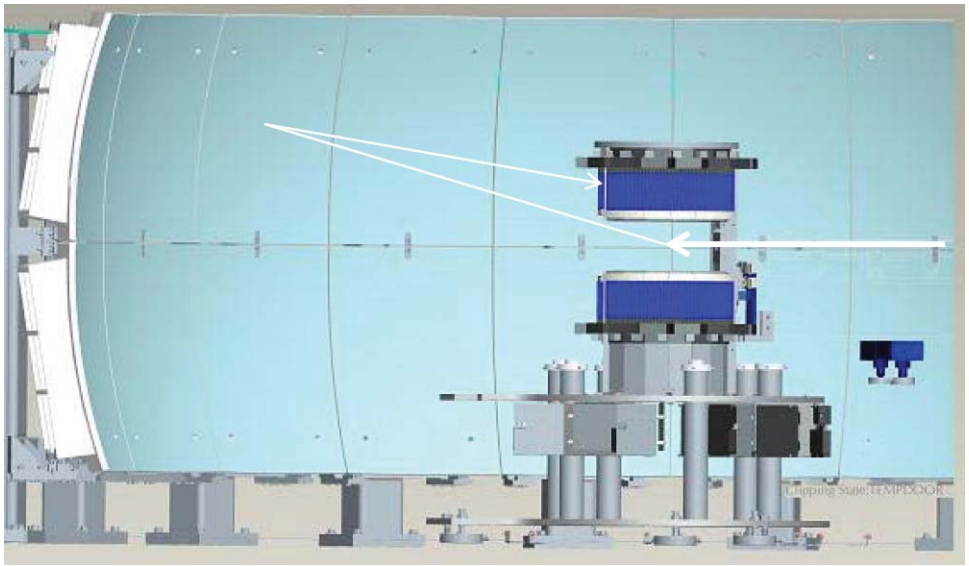

FIG. 4. (Color online) Schematic picture of the BASIS tank and the trajectory of a neutron (white arrows) that is scattered by the sample at the center, then Bragg-reflected by Si(111) analyzer crystals, and finally intercepted by a detector array. Neutrons reflected by the top and bottom sets of analyzer panels are detected in the top and bottom circles of the He-3 tubes, respectively. Not shown for clarity are the radial collimator, neutron guide, and background shielding.

FIG. 5. (Color online) Photograph of the Si(111) crystal analyzer panels inside the BASIS tank.

FIG. 6. (Color online) Photograph of the He-3 linear position-sensitive detector banks inside the BASIS tank, with the sample chamber, radial collimator and shielding removed for clear view. Also visible is the neutron guide in the horizontal plane, at midpoint height between the upper and lower detector banks.

crystals. However, here we discuss the performance of the BASIS in the present configuration that uses the original set of 18 Si(111) analyzer panels on one side of the instrument tank. The Q-averaged data for a vanadium standard of annular geometry presented in Fig. 8 shows a resolution of approximately 3.5 μeV (FWHM). On the negative energy transfer side (longer TOFs), there is additional broadening visible mostly on the linear intensity scale; this is a well-known and expected effect due to the moderator emission spectrum. On the logarithm intensity scale, there is additional broadening visible at the footstep of the elastic peak on the positive energy transfer side. This broadening originates from the specific design of the existing analyzer panels, and may be eliminated in the future panels, thus providing a sharper edge of the resolution peak at $E > 0$. Fig. 8 also demonstrates the signal-to-background ratio at the elastic line achieved to date, which well exceeds 1000:1. Again, this ratio is expected to increase even further with the introduction of the improved analyzer Si(111) panels. Importantly, the BASIS possesses an excellent energy resolution at the inelastic energy transfers (of about 0.1% of E_i), which makes possible high-resolution measurements of various excitations within the Q-ω region shown in Fig. 7. The Q-resolution of the BASIS, when operated in quasielastic regime, varies from about 0.1 Å^{-1} at the low scattering angles to about 0.05 Å^{-1} at the high scattering angles.

Figure 9 shows QENS spectrum ($Q = 0.7$ Å^{-1}) collected from a room-temperature ionic liquid, $[H_2NC(dma)_2][BETI]$.[15] Hydrogen-bearing liquid and powder samples that yield predominantly incoherent scattering signal are studied on the BASIS most often. The sample was loaded in a 0.1 mm thick annular cylindrical aluminum container 29 mm in diameter, 54 mm in height and measured at 320 K for about 4 hours. The SNS power at the time was about 0.4 MW. The data shown in Fig. 9 are plotted using 2 μeV energy binning. The presence of an asymmetric background, discussed in detail in Ref. 15, is evident in both the data and fits. Importantly, the wide dynamic range of the experiment was instrumental in comparing between different

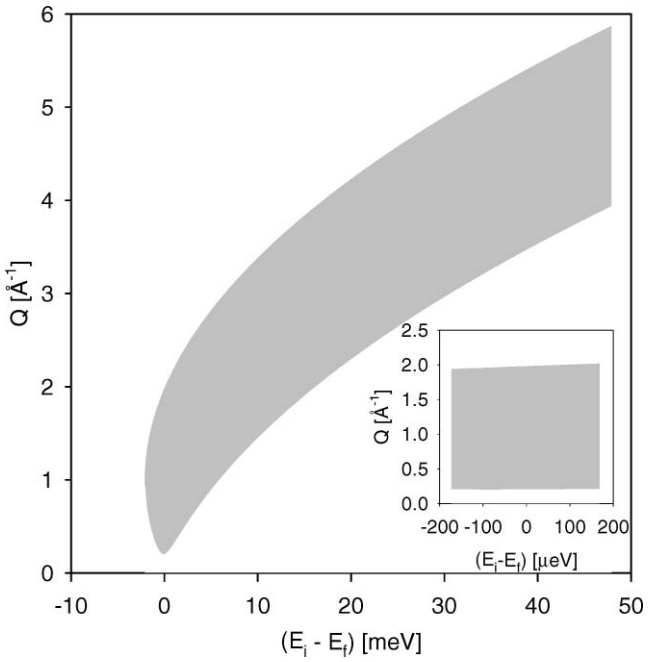

FIG. 7. Q-ω region accessible on the BASIS. Inset: Q-ω coverage in quasielastic regime at 60 Hz.

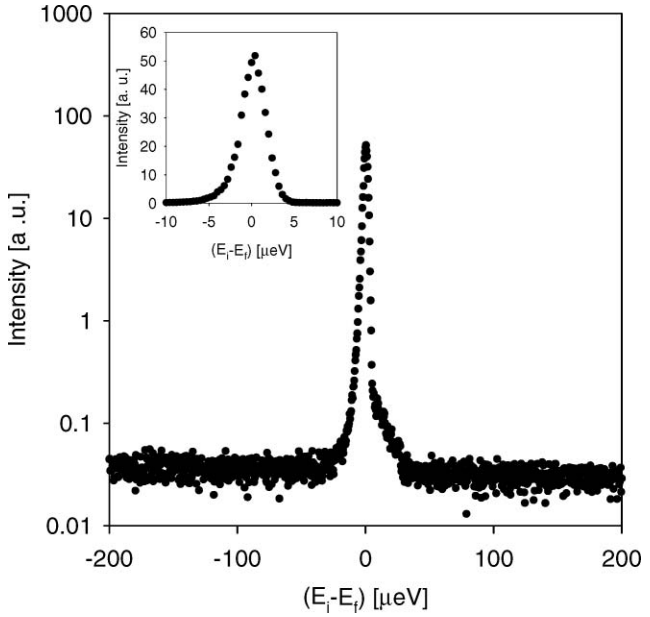

FIG. 8. Q-averaged spectrum collected from a 10% scattering annular vanadium standard showing the signal-to-noise ratio and the energy resolution of about 3.5 μeV (inset) of the BASIS.

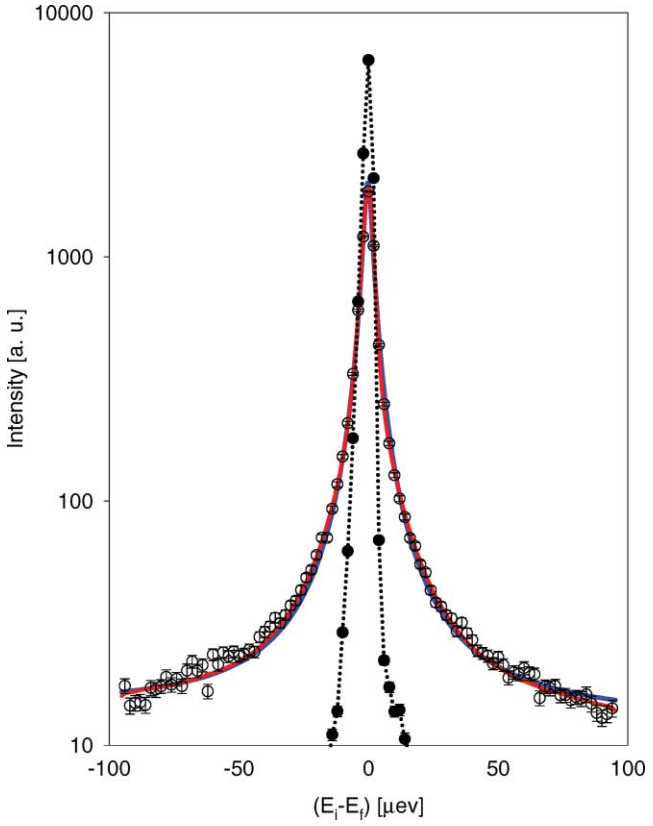

FIG. 9. (Color) Open symbols: QENS spectrum ($Q = 0.7$ Å^{-1}) of a room-temperature ionic liquid, $[H_2NC(dma)_2][BETI]$, measured on the BASIS at 320 K.[15] The resolution spectrum measured from the same sample at 7 K is shown with the filled symbols and dotted line. Solid lines are fits using an asymmetric background and the resolution-convolved model scattering function in the form of two Lorentzians (red) and a Fourier-transformed stretched exponential (blue).

model scattering functions that both yield reasonable fits, yet represent very different scenarios of diffusion processes.

While the Q-averaged energy resolution value for an annular sample with standard dimensions is about 3.5 μeV, as shown in Fig. 8, we have found a significant dependence of the resolution on Q (essentially, the scattering angle). The best resolution is achieved at the lowest scattering angles, whereas the highest scattering angles are associated with the coarsest resolution. This is an effect due to the sample geometry-dependent correlations between the incident and final flight paths, L_i and L_f, which is not predicted by Eqs. (3)–(8) that assume independent distributions of various uncertainties around their mean values. In reality, the flight path lengths are somewhat correlated, as explained schematically in Fig. 10, leading to the Q- (or angular) dependence of the resolution function for an annular sample. Assuming that the incident neutrons with $\lambda = 6.267$ Å arrive simultaneously and with no divergence at the plane that contains the point U and is perpendicular to the incident beam direction, the total time-of-flight from this plane to the analyzers that are much far away from the sample will vary depending on the direction of the scattered neutrons. For the forward-scattering direction ($2\theta = 0^\circ$), the arrival time at the analyzer would be the same for the neutron scattered elastically from the sample at the points U, D, R, and L. For the scattering at $2\theta = 90^\circ$, the neutrons scattered at the points U and L will arrive at the analyzer first, followed by the neutrons scattered at the points R and D, which will be delayed by $t = D$/v, where D is the sample diameter, and v is the neutron velocity. An even bigger spread will be seen for the neutrons scattered in the back-scattering direction ($2\theta = 180^\circ$); the neutrons scattered at the point U will arrive at the analyzer first, followed by the neutrons scattered at the points L and R and delayed by $t = D$/v, followed by the neutrons scattered at the point D and delayed by $t = 2D$/v with respect to the neutrons scattered at the point U. Thus, the resolution is expected to worsen at higher scattering angles, as observed experimentally.

Similar effect is known for the direct geometry TOF spectrometers as well, where the neutrons arriving directly at the detectors following scattering from the sample experience a larger spread of arrival times at higher scattering angles. The relative strength of this effect should depend on the characteristic TOF of the scattered neutrons through the sample. For the BASIS, with a typical annular sample diameter of 2.9 cm and the neutron velocity at the elastic line of 630 m/s, the characteristic TOF through the sample, D/v, is about 46 μs. This is comparable with the other leading contributions to the overall resolution, such as the 60 μs moderator emission time width, so the angular resolution dependence is quite pronounced. On the other hand, a flat-plate sample with a 45° orientation of its normal (that is, 135° orientation of its plane) with respect to the incident beam on the BASIS yields almost Q-independent resolution of about 3 μeV (FWHM) for the scattering angles up to $2\theta = 90^\circ$; this is a well-known geometry focusing effect.

When the SNS power was about 0.5 MW, measurement of the incident neutron flux at the sample position in quasielastic regime (choppers at 60 Hz, 0.5 Å incident wavelength band centered at 6.4 Å) yielded a value of about

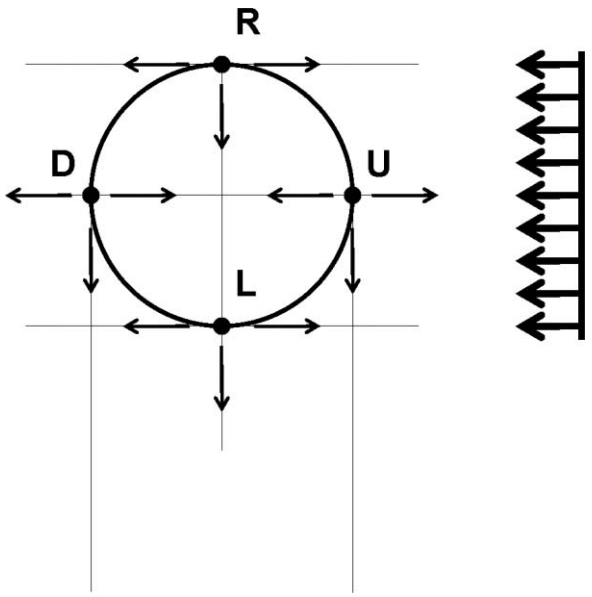

FIG. 10. A schematic explanation of the Q- (or angular) dependence of the resolution function for an annular sample. A two-dimensional picture of the scattering in the horizontal plane is shown for simplicity for 4 points on the sample: upstream (U), downstream (D), right (R), and left (L), with respect to the incident beam). The spread in the arrival time at the analyzers grows with increasing scattering angle, as explained in the text.

1.3×10^7 n/cm^{2}s. More practically important are the data collection rates; with a vanadium standard of 94% transmission, the count rate of about 25 ct/sec (integrated over all detectors) was obtained in the elastic time-of-flight channel of a 10 μs width, which corresponds to 0.4 μeV width of an energy transfer bin at the elastic line. The raw data collected from standard annular vanadium samples in 5 minutes and integrated over all detector pixels are shown in Fig. 11 as counts

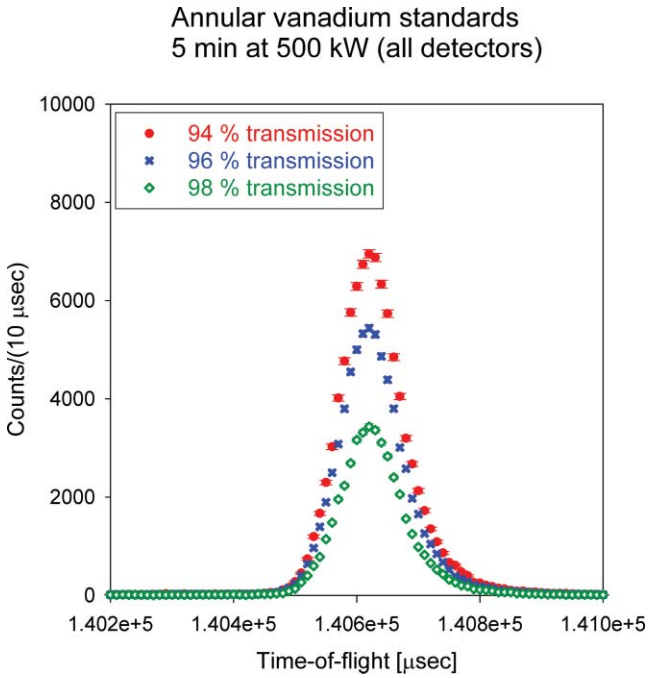

FIG. 11. (Color online) Raw data as a function of time-of-flight for annular vanadium samples of standard dimensions with different transmissions collected in 5 minutes at 500 kW beam power.

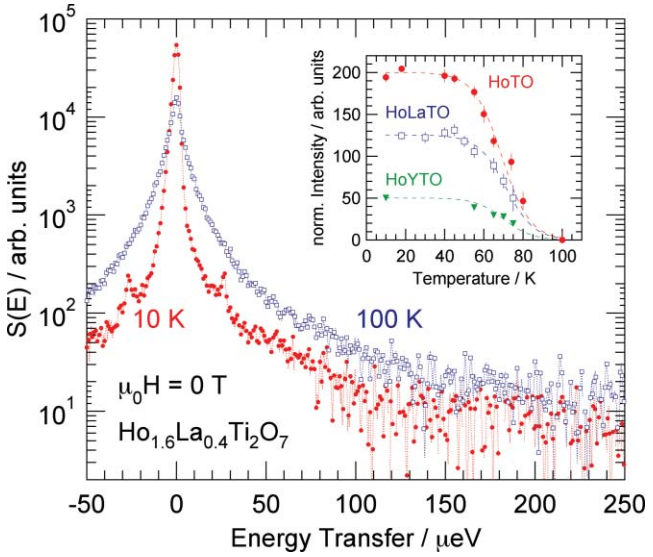

FIG. 12. (Color online) Scattering intensities measured on the BASIS in zero magnetic field for $Ho_{1.6}La_{0.4}Ti_2O_7$ and other holmium-bearing samples.[16] Note sharp excitations at ±26.3 μeV visible in the 10 K spectrum.

per 10 μs TOF channels. The projected power of the SNS (not considering possible future upgrades) is 1.4 MW; thus, an improvement in the data collection rate by almost a factor of 3 can be expected.

Recent studies of a spin ice compound $Ho_2Ti_2O_7$ and its derivatives[16] provide a good illustration of the current BASIS capabilities, as shown in Fig. 12. In addition to the strong quasielastic signal, one can see the sharp excitations at ±26.3 μeV that were attributed to the transitions between nuclear spin states of Ho split by the hyperfine field.[16] The BASIS possesses simultaneously the high energy resolution and relatively large dynamic range, as well as the high signal-to-noise ratio that is more than sufficient to resolve these weak (less than 0.2% of the elastic intensity) excitations.

With its high energy resolution and a variable dynamic range, BASIS is, perhaps, the first operating instrument that provides an excellent overlap between quasielastic neutron scattering (QENS) measurements carried out on the inverted-geometry backscattering and direct-geometry time-of-flight cold neutron spectrometers. At the SNS, complementary QENS measurements are possible with the cold neutron chopper spectrometer, CNCS, which will typically provide an energy resolution between 10 and 500 μeV.

ACKNOWLEDGMENTS

The design, construction, and commissioning of the BASIS have been the result of efforts of many scientists, engineers, technicians, programmers, and other personnel at the ORNL's Spallation Neutron Source. The authors are deeply thankful to all those who contributed to the successful construction and operation of the spectrometer. We are grateful to M. Hagen and M. Zamponi for fruitful discussions. The operation and user program at the SNS is supported by the Scientific User Facilities Division, Office of Basic Energy Sciences, (U.S.) Department of Energy (DOE).

[1]H. Maier-Leibnitz, Nukleonik **8**, 61 (1966).
[2]B. Alefeld, Bayrische Akad. Wiss., Math.-Naturwiss. Kl. **11**, 109 (1967).
[3]J. C. Cook, W. Petry, A. Heidemann, and J.-F. Barthelemy, Nucl. Instrum. Methods Phys. Res. A **312**, 553 (1992).
[4]M. Birr, A. Heidemannn, and B. Alefeld, Nucl. Instrum. Methods **95**, 435 (1971).
[5]B. Frick, A. Magerl, Y. Blanc, and R. Rebesco, Physica B **234-236**, 1177 (1997).
[6]A. Meyer, R. M. Dimeo, P. M. Gehring, and D. A. Neumann, Rev. Sci. Instrum. **74**, 2759 (2003).
[7]See http://www.jcns.info/jcns_spheres for information on the SPHERES spectrometer.
[8]K. Inoue, T. Kanaya, Y. Kiyanagi, S. Ikeda, K. Shibata, H. Iwasa, T. Kamiyama, N. Watanabe, and Y. Izumi, Nucl. Instrum. Methods Phys. Res. A **309**, 294 (1991).
[9]S. Ikeda, N. Watanabe, K. Inoue, Y. Kiyanagi, A. Inaba, S. Takeda, T. Kanaya, K. Shibata, T. Kamiyama, Y. Izumi, Y. Ozaki, and C. J. Carlile, J. Phys. Soc. Jpn. **60**, 3340 (1991).
[10]C. J. Carlile and M. A. Adams, Physica B **182**, 431 (1992).
[11]M. T. F. Telling, S. I. Campbell, D. D. Abbley, D. A. Cragg, J. J. P. Balchin, and C. J. Carlile, Appl. Phys. A **74**, S61 (2002).
[12]M. T. F. Telling and K. H. Andersen, Phys. Chem. Chem. Phys. **7**, 1255 (2005).
[13]See http://sns.gov/instruments/SNS/BASIS/ for information on the BASIS spectrometer.
[14]K. W. Herwig and W. S. Keener, Appl. Phys. A: Mater. Sci. Process. **74**, S1592 (2002).
[15]E. Mamontov, H. Luo, and S. Dai, J. Phys. Chem. B **113**, 159 (2009).
[16]G. Ehlers, E. Mamontov, M. Zamponi, K. C. Kam, and J. C. Gardner, Phys. Rev. Lett. **102**, 016405 (2009).